CrossMark

Dip-coating deposition of BiVO$_4$/NiO p–n heterojunction thin film and efficiency for methylene blue degradation

M. R. da Silva[1,2] · L. V. A. Scalvi[2] · Vanildo Souza Leão Neto[3] · L. H. Dall'Antonia[3]

Abstract This paper deals with a simple FTO/p–n heterojunction electrode assembly formed by BiVO$_4$ and NiO thin films, where the precursor solution is obtained by solution combustion synthesis and precipitation in aqueous media techniques, respectively, whereas the thin films were deposited by the dip-coating deposition process. The FTO/p–n electrodes are characterized by X-ray diffraction, scanning electron microscopy, Raman spectroscopy and UV–Vis spectroscopy. The performance analysis based on the methylene blue degradation reaction have shown that the p–n electrodes, FTO/p-NiO/n-BiVO$_4$ and FTO/n-BiVO$_4$/p-NiO have higher electroactivity under visible light irradiation condition when compared to single BiVO$_4$ thin film, deposited separately, with estimated k_{obs} value of 340×10^{-4} min^{-1}, 270×10^{-4} min^{-1} and 150×10^{-4} min^{-1}, respectively.

1 Introduction

The recent stage of environmental degradation has led the World population to become aware and somehow fighting for the natural environment preservation. The "sustainability" term is becoming increasingly common in public policy proposals from all over the World. It shows the great global concern with the preservation of the environment, and thus has provided the development and encouragement of scientific projects guided by sustainability. In this context, the development of new technologies and new materials that may be used in preserving and protecting the environment, has become an increasing interest issue [1, 2].

Photocatalysis and photoelectrocatalysis are potential tools to treat the environmental preservation problem, more specifically in decontaminating wastewater. To accomplish that, it may be used a photoactive semiconductor material such as TiO$_2$ [3, 4] or ZnO [5, 6]. One of the main problems of photocatalysis is the recombination process of photogenerated electron–hole pairs, which greatly limits the use of such methodology. In the photoelectrocatalysis, the effect of recombination process is minimized by the action of the applied potential to the system, forcing the flow of photogenerated electrons to the counter-electrode. However, the applying potential does not guarantee the complete inhibition of recombination, where a small recombination percentage of photogenerated electron–hole pairs takes place, leading to a slightly decrease in the technique efficiency [7–9].

The combination of photoactive semiconductor materials as heterojunctions seems to be an interesting approach, where a well designed interface may lead to photoinduced charge separation and the suppression of electron–hole recombination. Heterojunctions using transparent oxides deposited on top of traditional semiconductors have been presented recently, with many sort of applications. High-quality ZnO films have been grown on top of GaAs, forming a heterojunction with characteristic of rectifying diode, with blue-violet and infrared electroluminescence [10], suitable for optical fiber telecommunications applications. Promising devices for the development of solid-state lighting were achieved by n-ZnO/n-GaAs heterostructured light-emitting

✉ M. R. da Silva
marcelors@feb.unesp.br

1 Engineering College, CTI, UNESP – São Paulo State University, Bauru, SP, Brazil

2 Department of Physics – FC, UNESP –São Paulo State University, Bauru, SP, Brazil

3 Department of Chemistry, UEL – State University of Londrina, Londrina, PR, Brazil

diodes [11]. The combination of SnO$_2$ with Al$_2$O$_3$ layer deposited by a combination of simple techniques: dip-coating/resistive evaporation respectively, has led to a device with potential application as transparent transistors [12].

The deposition of heterojunctions with smooth and atomic quality surfaces has become a possibility since the late 60s, when the growth of epitaxy layers became available. This sort of deposition may lead to the formation of a quantum well at the interface, due to the interrupting atomic band diagrams of distinct materials. This quantum well may present energy levels below the conduction band bottom of one or both materials and, may give birth to a two-dimensional electron gas (2DEG). The interface of semiconductor heterojunctions carries intrinsic states, and the Fermi level at the surface is different from the bulk, giving origin to a band bending [13]. A triangular quantum well forms at the semiconductors interface, usually referred to as the heterointerface. Normally, only the quantum mechanical ground state in the triangular well is populated, but the excited levels can be filled with the application of an electric field. A 2DEG has recently been also found at the interface between two insulating oxides LaAlO$_3$ and SrTiO$_3$ [14], attracting significant interest due to possible applications in all-oxide electronic devices, and has stimulated intense research activity in this field. Other similar publications related to 2DEG formation can also be found in the recent literature [15, 16]. SnO$_2$/GaAs heterojunctions thin films deposited by similar procedure as used in this paper have been successfully obtained, giving birth to smooth interface and improved electrical properties [17, 18].

Positive–negative (p–n) heterojunctions emerge as interesting strategy to suppression of electron–hole pairs recombination effect and increase of the quantum efficiency [19–22]. Besides, an appropriate combination of p–n layers may lead to advantages concerning the photo-excitation. For instance, photo-excitable semiconductor materials have advantages compared to other materials when they can be excited by visible light, because the sunlight is available to be used, reducing operating costs in a practical application. Moreover, it must necessarily be chosen a non-toxic material to human health, presenting high chemical stability, including high photocorrosion resistance [23–25]. Considering the non-toxicity and high chemical stability, the semiconductors BiVO$_4$ and NiO have been extensively studied in isolated form. They also have been used to form p–n junctions with other semiconductors. In both cases, they have used in the degradation of organic compounds in aqueous medium [19, 22–27]. Zhang et al. [21] evaluated the photocatalytic properties of TiO$_2$/BiVO$_4$ composite photocatalysts synthesized by the one-step microwave hydrothermal method, and showed that this combination has higher photocatalytic

activity in the rhodamine B degradation when compared to pure BiVO$_4$. In other paper, Wang et al. [27] prepared Cu$_2$O/BiVO$_4$ p–n junction through coupling a hydrothermal process with polyol strategy. The higher photocatalytic activity for the methylene blue degradation is due an effective reduction in the recombination of electron–hole pair by p–n junction than pure BiVO$_4$ and Cu$_2$O. More recently, Zhang et al. [20] evaluated the photocatalytic properties of CuO/BiVO$_4$ composite photocatalysts prepared by modified metalorganic decomposition and impregnation methods, respectively, and the results have shown that 5 wt% CuO on BiVO$_4$ surface leads to the highest photocatalytic activity for methylene blue degradation reaction. The heterojunction of BiVO$_4$ and NiO, discussed in this work, has been reported a few times, but with samples in different shapes [22] compared to the format reported here.

Considering that the combination of BiVO$_4$ with NiO as a p–n junction is not properly studied in the literature so far, the present work deals with a simple and efficient methodology for obtaining thin films of p-NiO/n-BiVO$_4$ heterojunctions deposited on fluor-doped tin dioxide (FTO) substrate. The main goal is to demonstrate that the electrode formed by this p–n junction exhibits higher photocatalytic activity towards the methylene blue dye degradation reaction when compared to these semiconductor materials deposited in an isolated way. Besides the role of the interface phenomena is investigated concerning the suppression of electron–hole recombination. The results show that this p–n heterostructure within a specific architecture emerges as a potential electrode material that can be used in a real situation of decontaminating wastewater.

2 Experimental

2.1 Synthesis of n-BiVO$_4$ and p-NiO semiconductor solutions

The BiVO$_4$ n-type semiconductor precursor was obtained by the solution combustion synthesis (SCS) technique, adapted from widely published procedures [7, 9, 28–30]. First, a bismuth precursor solution was prepared by adding 2.4 g of Bi (NO$_3$)$_3$·6H$_2$O (Sigma-Aldrich, p.a.) and 1.0 g of citric acid (Sigma-Aldrich, p.a.), which were dissolved in 100 mL of 1.5 mol L^{-1} HNO$_3$ (Sigma-Aldrich, p.a.), leading to a colorless solution. Then, the pH of this solution was adjusted to 7–8 by dripping concentrated ammonium hydroxide. Finally, 2 g of urea was added to this solution, which plays the role of combustible for the self-sustainable reaction of the SCS technique [29–31]. The synthesis process was continued through the preparation of the

vanadium precursor solution by adding 1.0 g of citric acid and 0.6 g of $(NH_4)_3VO_4$ (Sigma-Aldrich, p.a.), which was dissolved in 100 mL of deionized water at 80 °C, remaining under stirring for 20 min, originating a yellowish solution. The colorless and yellowish solutions were mixed together and left in a muffle oven at 85 °C for 20 h, giving birth to a material with gel consistency and intense green color. This green gel was diluted in 50 mL of deionized water, resulting in a greenish solution that was called solution "A", which was used as precursor solution for the $BiVO_4$ thin film deposition.

The NiO p-type semiconductor solution was obtained by precipitation in aqueous media, also adapted from widely published procedures [32–34]. Firstly, 100 mL of 0.5 mol L^{-1} $Ni(NO_3)_2{\cdot}6H_2O$ (Sigma-Aldrich) was prepared. Then, its pH was adjusted to 7–8 by the slowly addition of concentrated NH_4OH (Merck). This condition assures the precipitation of $Ni(OH)_2$, because its K_{PS} is 5.46×10^{-16}, yielding a green opaque colloidal suspension with $Ni(OH)_2$ particles, that was called solution "B". This solution "B" was used for deposition of NiO thin film on p–n junction electrode.

2.2 Construction of p–n junction on FTO electrode

The procedure to obtain the p–n junction electrodes is illustrated in the diagram of Fig. 1. The solution "A" was used to deposit $BiVO_4$ thin film on Fluor-doped tin oxide (FTO) conductor substrate, where the substrate is sequentially dipped according to the desired number of layers, by using the dip rate of 10 cm/min. Between each deposited layer, the sample is dried for 10 min in room atmosphere, followed by heating at 300 °C for additional 10 min. When the desired number of layers is reached (in the present case it corresponds to ten layers), the film is thermally annealed at 400 °C for 4 h. The same procedure was utilized to deposit NiO thin film, using the solution "B". Two electrodes were confectioned as follows: (1) ten layers of $BiVO_4$ deposited on FTO substrate, followed by ten layers of NiO deposited on top of the $BiVO_4$ film, forming the FTO/n-$BiVO_4$/p-NiO electrode. (2) Ten layers of NiO deposited on FTO substrate, followed by ten layers of $BiVO_4$ deposited over NiO, forming the FTO/p-NiO/n-$BiVO_4$ electrode.

2.3 Thin film heterojunction characterization

X-ray diffraction (XRD) measurements were carried out using a PANalytical diffractometer, model X'Pert PRO MPD, with the CuKα (1.5418 Å) radiation, coupled to a nickel filter, in order to reduce the unfavorable CuKβ radiation. The applied tension was 40 kV and the current was 30 mA. The scanning range was from 10° to 80°, with regular step of 0.05° s^{-1}. Scanning electron microscopy (SEM) images were obtained in a Quanta 200-FEI microscope with 30 kV of applied voltage. Raman scattering data were obtained by a Bruker FT, model Raman RFS 100 spectrometer, with excitation at 1,064 nm, obtained through the Nd:YAG laser of 200 mW. The scanning system works with accumulation of 256 scans and 2 cm^{-1} spectral resolution.

2.4 Methylene blue degradation test

The methylene blue (MB) degradation test was carried out by chronoamperometry technique, with controlled potential
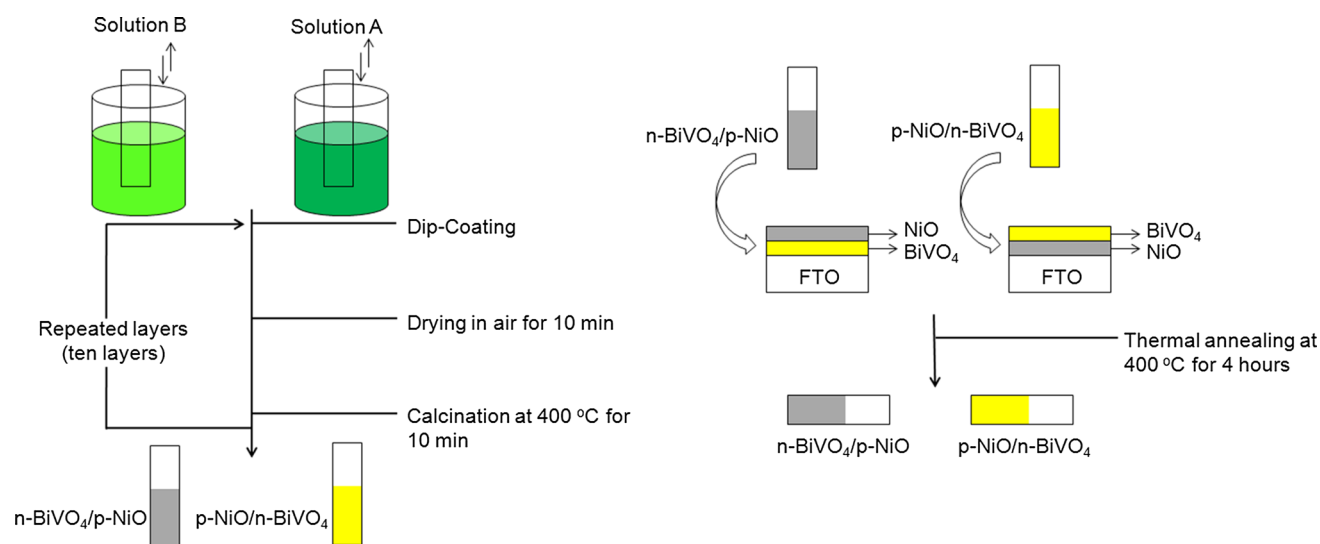

Fig. 1 Simplified diagram showing the dip-coating deposition process to obtain p–n heterojunction electrodes

of +1.4 V during different degradation times in 0.1 mol L^{-1} KCl electrolyte solution. A conventional one compartment electrochemical cell with three electrodes were used for the degradation experiments, where an Ag/AgCl (1 mol L^{-1} KCl) electrode was used as reference electrode, a platinum wire (10 cm long and 0.5 mm of diameter) was the counter-electrode, and the p–n junction electrode, deposited on fluorine-doped tin oxide (FTO conductor substrate, as just described in the previous section), was used as working electrode (the geometrical electrode area in contact with the solution is set to 1 cm^2). The light irradiation in the electrochemical system is done through a Philips dichroic lamp with a power of 50 W at an applied voltage of 12 V. This light source presents wide spectra, with emission from $\lambda \geq 400$ nm. It must be mentioned that illumination was done in the front part of the p–n junction electrode. A potentiostat/galvanostat AUTOLAB 84057, version 4.9, was used for data collecting. After degradation, UV–Vis spectra of the remaining solution were taken and used to verify the relative (percentage) amount of MB that had vanished. The adopted parameter was the decreasing of the MB optical absorption band maximum, taken at approximately 665 nm. These spectra were taken just after the chronoamperometry measurements.

3 Results and discussions

The X-ray results obtained from NiO, BiVO$_4$, NiO/BiVO$_4$ and BiVO$_4$/NiO film samples, which are called here as sample 1, 2, 3 and 4, respectively, are shown in Fig. 2. In all diffractograms it is possible to observe the diffraction peaks of the FTO substrate. The diffracted peaks in sample 1 at about $2\theta = 37.3°$, $43.2°$ and $63.4°$, associated with the crystallographic planes (111), (200) and (220), are due the
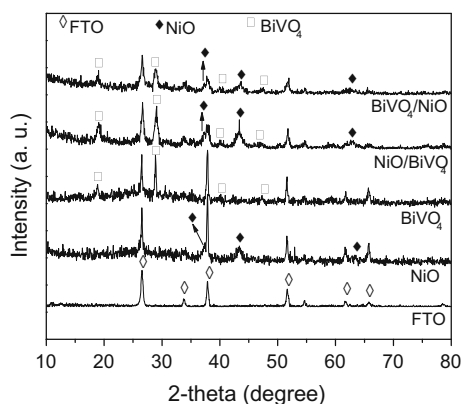
face-centered cubic (fcc) phase of NiO with spatial group Fm-3 m (225) and lattice parameter a = 4.177 Å, as obtained by comparison with the crystallographic pattern (PCPDFWIN software, version 2.4, JCODS-ICDD, card 65-5745). The diffracted peaks in sample 2 at about $2\theta = 18.7°$, $28.8°$, $40.2°$ and $47.2°$, associated with the crystallographic planes (011), (112), (211) and (024), are due the monoclinic phase of BiVO$_4$ that belongs to spatial group I2/b, with lattice parameters a = 5.195 Å, b = 5.093 Å, and c = 11.704 Å (card 83-1699 of the same mentioned software). In the diffractograms of samples 3 and 4 it is possible to observe a mixed of the fcc NiO and monoclinic BiVO$_4$ phases (as marked with symbols at the diffracted peaks). Then, it is clearly shown that both phases are present, besides we believe that regions of mixed phase may take place on sample surface, due the prolonged thermal annealing time, as previously discussed in another paper [7]. Images of SEM, as shown in the upcoming discussion, evidence that.

SEM images of films containing only the material NiO and only BiVO$_4$ with ten deposited layers on FTO substrate are seen in Fig. 3. The image of the NiO film surface (Fig. 3a) is rather homogeneous, but with different particles format, being formed of intermingled plates randomly distributed mixed with some round-shaped particles. The image of the BiVO$_4$ film surface (Fig. 3b) is also quite homogeneous, being formed of round-shaped particles uniformly distributed throughout the investigated area. SEM images with different magnifications of p–n heterojunctions thin films deposited on FTO substrate are seen in Fig. 4. Figure 4a–c correspond to FTO/n-BiVO$_4$/p-NiO (as described on the experimental procedure), where the shown images of the n-p heterojunction surface are similar to the NiO surface (Fig. 3a), with intermingled plates randomly distributed mixed with some round-shaped particles. The distribution of particle formats is rather irregular in Fig. 4a–c, in good agreement with the image shown in 3a, of single NiO film. The Fig. 4d–f correspond to the p–n heterojunction sample FTO/p-NiO/n-BiVO$_4$. In this former case, the images allow seeing particles with different size and irregular shape, some spherical and others with non-defined shape. Moreover, the different size and irregular shape of BiVO$_4$ particles over NiO thin film or vice versa, which is more pronounced when NiO is the top layer, leads to non-homogeneous surface with deep regions formed by NiO channels surrounded by BiVO$_4$ aggregate particles or vice versa. Looking at Fig. 4a, b, it seems that both sort of materials show up at heterojunction surface, justifying the presence of both peaks at Fig. 2 (XRD). Although it may be an undesirable effect for an electronic device, it may be very useful for photoelectrocatalysis electrode design, because this non-uniformity on the surface distribution leads to a high roughness surface which implies in a higher
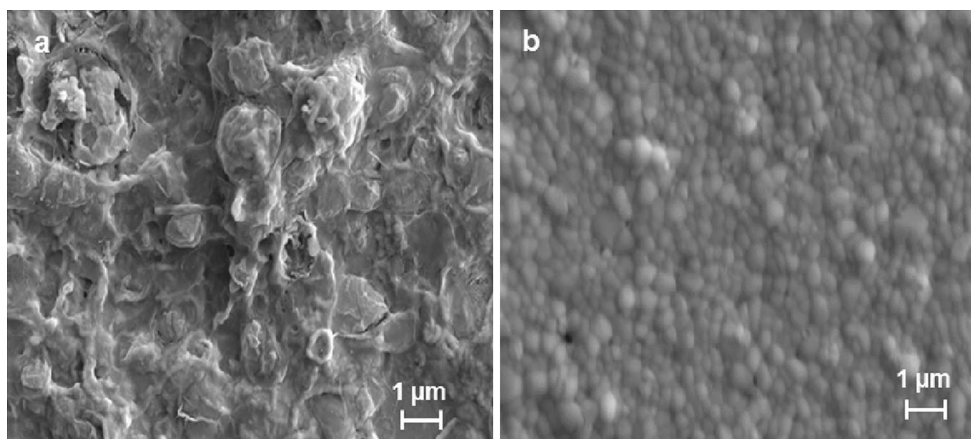
Fig. 2 X-ray diffractogram of samples 1, 2, 3 and 4 (NiO, BiVO$_4$, p-NiO/n-BiVO$_4$ and n-BiVO$_4$/p-NiO, respectively) deposited on FTO substrate

Fig. 3 SEM surface images of single **a** NiO and **b** BiVO$_4$ thin films with ten deposited layers on FTO substrate

surface area. This characteristic leads to a higher adsorption of molecules in the deeper channels, which means greater efficiency in the photoelectrocatalytic system.

The Raman spectra of BiVO$_4$ and NiO samples, deposited as isolated thin films, and p–n heterojunction film samples, deposited on FTO substrate, are shown in Fig. 5. In the Raman spectra of single BiVO$_4$ film four peaks are observed: about 830 and 708 cm^{-1} corresponding to symmetric and asymmetric stretching of vanadium–oxygen bound, respectively, and about 372 and 326 cm^{-1} are related to the symmetric and asymmetric deformations of VO$_4^{-3}$ group, respectively. This result is in good agreement with some published reports [35–37]. Concerning the Raman spectra of single NiO film five peaks are observed. According to Mironova-Ulmane et al. [38] and Marciuš et al. [39] the typical Raman scattering on nickel oxide films are a result of one and two-phonon excitations as well as two-magnon excitations. The peak at about 1480 cm^{-1} corresponds to two-magnon (2 M) band F excitations [38, 40]. Raman peaks located at 540 and 410 cm^{-1} correspond to nickel–oxygen stretching mode [41, 42], assigned to the first order transverse optical (TO) and longitudinal optical (LO) phonon modes of NiO thin film, respectively, which are in good agreement with reported values by Gowthami et al. [42] and Xu et al. [43]. The peaks at 1100 and 723 cm^{-1} are due the two-phonon 2LO and 2TO modes [39]. About the p–n junction, NiO/BiVO$_4$ thin film, it is possible to observe the characteristic peaks of single NiO and BiVO$_4$. These results are in very good agreement with XRD and SEM results, previously discussed, where was possible to identify diffraction peaks of the two material and observe a mixtures of NiO and BiVO$_4$ phases in the samples surfaces. These features are probably caused due the prolonged thermal annealing time.

UV–Vis optical absorption data for samples 1, 2, 3 and 4 are shown in Fig. 6. The absorption edge of sample 1

(Fig. 6a), corresponding to NiO film alone, occurs at about 350 nm, UV region, typical of this semiconductor material [34, 44]. The inset in Fig. 6a shows the bandgap energy evaluation, considering direct bandgap transition for NiO [44], where the plot of $(\alpha h\nu)^2$ versus ($h\nu$) yields a bandgap of 3.4 eV. The absorption edge of sample 2 (Fig. 6b), corresponding to BiVO$_4$ film, occurs at about 515 nm in the visible light region with a bandgap energy value of 2.4 eV (inset in Fig. 6b). This bandgap value is typical of monoclinic BiVO$_4$ material [7, 9, 29, 30, 35]. The UV–Vis spectra of the heterojunction materials, samples 3 and 4, corresponding to p–n NiO/BiVO$_4$ and n–p BiVO$_4$/NiO films, are shown in Fig. 6c, d, respectively. It is possible to observe that the absorption edge is similar for both samples, with higher energy compared to BiVO$_4$ film and lower energy compared to NiO film. The inset of Fig. 6c, d correspond to bandgap evaluation for the heterojunction samples, considering direct bandgap transition, since this is the case for both semiconductor materials. A small shift in the position of fundamental absorption edges of p–n junction, compared to single BiVO$_4$, is observed, leading an increase of the bandgap energy, with slightly different values of 2.55 and 2.59 eV to samples 3 and 4, respectively. The observed behavior is typical of p–n junction materials, as discussed in some papers [19, 20, 22–25, 45].

Figure 7 shows UV–Vis absorption spectra of the MB solution after photoelectrochemical degradation with single BiVO$_4$ film (Fig. 7a), and with the p–n junction films, BiVO$_4$/NiO (Fig. 7b) and NiO/BiVO$_4$ (Fig. 7c), in 0.1 mol L^{-1} KCl electrolyte. The electrolysis was carried out by chronoamperometry with +1.4 V versus Ag/AgCl controlled potential, under visible light irradiation condition, where it was used a Philips dichroic lamp. It is possible to observe that both materials are electroactives face to the MB degradation as verified by the decrease of absorption band of MB measured at about 655 nm.
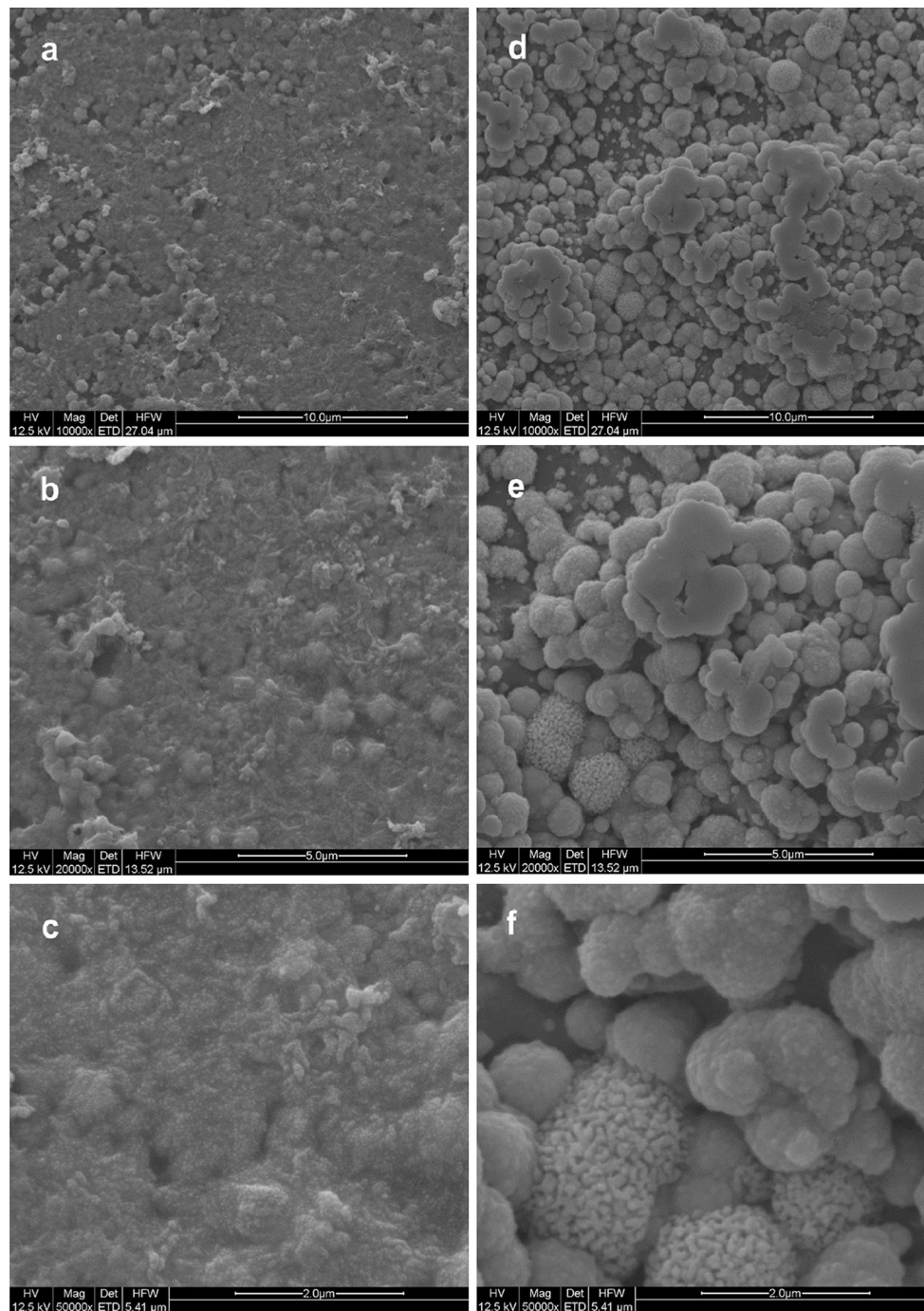
Fig. 4 SEM images with different magnifications of heterojunctions thin films deposited on FTO substrate: **a–c** FTO/n-BiVO$_4$/p-NiO and **d–f** FTO/p-NiO/n-BiVO$_4$

However, the p–n junction electrodes configurations have shown electrocatalytic activity higher than single BiVO$_4$, where 45 % of MB was decomposed by single BiVO$_4$ and 65 % and 75 % of MB was decomposed by BiVO$_4$/NiO and NiO/BiVO$_4$, respectively, for the same exposition time (40 min). Figure 7d shows the decrease of MB concentration as a function of reaction time. The decay profile of

the curves suggests that both processes follow first-order kinetics. The rate constant of the reaction (k_{obs}) can be easily evaluated, as widely published [7, 29, 30, 35]. The rate constant values obtained are also summarized in Table 1. The rate constant values to the single BiVO$_4$, NiO/BiVO$_4$ and BiVO$_4$/NiO are 150×10^{-4}, 340×10^{-4} and 270×10^{-4} min^{-1}, respectively. From these results, it

is observed that the rate constant of MB degradation by p–n function electrodes is higher than single $BiVO_4$ film. Due to the visible light spectra, used for the sample excitation, a comparison with the single NiO film sample is not adequate, because the NiO bandgap is about 3.5 eV, in the UV range, whereas the Philips dichroic excitation source presents emission from $\lambda \geq 400$ nm.
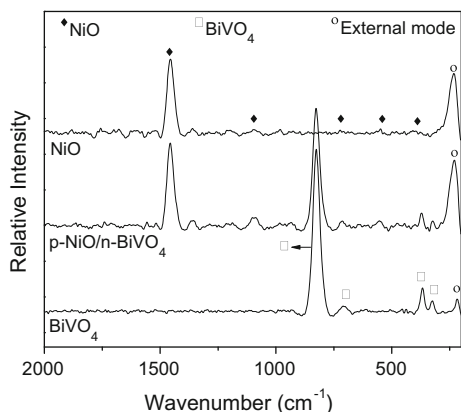

Fig. 5 Raman spectra of single NiO, pure $BiVO_4$ and p–n heterojunction thin films deposited on FTO substrate

Although the proposal is the integration of n-type $BiVO_4$ and p-type NiO layer-by-layer as thin films, as described in the experimental section, a rather distinct number of smaller p–n junctions were formed on surface of the heterojunction, as obtained from the results of XRD and SEM, as described previously. Therefore, Fig. 8a depicts the film surface as revealed by the results, showing a number of possible p–n junctions. In this illustrative design, yellow balls correspond to $BiVO_4$ material and the gray color in the background corresponds to NiO. So, based on the band-edge potential positions of these two semiconductors, we proposed a photoelectrocatalytic mechanism to explain the higher degradation percentage of MB by the p–n heterojunction electrode. The band-edge positions of the conduction band and valence band can be determined using the following empirical equation [21]:

$$E_{VB} = \chi - E^e + 0.5E_g \tag{1}$$

$$E_{CB} = E_{VB} - E_g \tag{2}$$

where E_{VB} is the valence band-edge potential position and E_{CB} is the conduction band-edge potential position, χ is the absolute electronegativity of the semiconductor (χ is 6.04 eV [46] and 5.91 eV [47] for $BiVO_4$ and NiO,

Fig. 6 UV–Vis optical absorption spectra of samples: **a** 1, **b** 2, **c** 3 and **d** 4 (NiO, $BiVO_4$, p-NiO/n-$BiVO_4$ and n-$BiVO_4$/p-NiO, respectively) deposited on FTO substrate. *Inset* bandgap energy evaluation
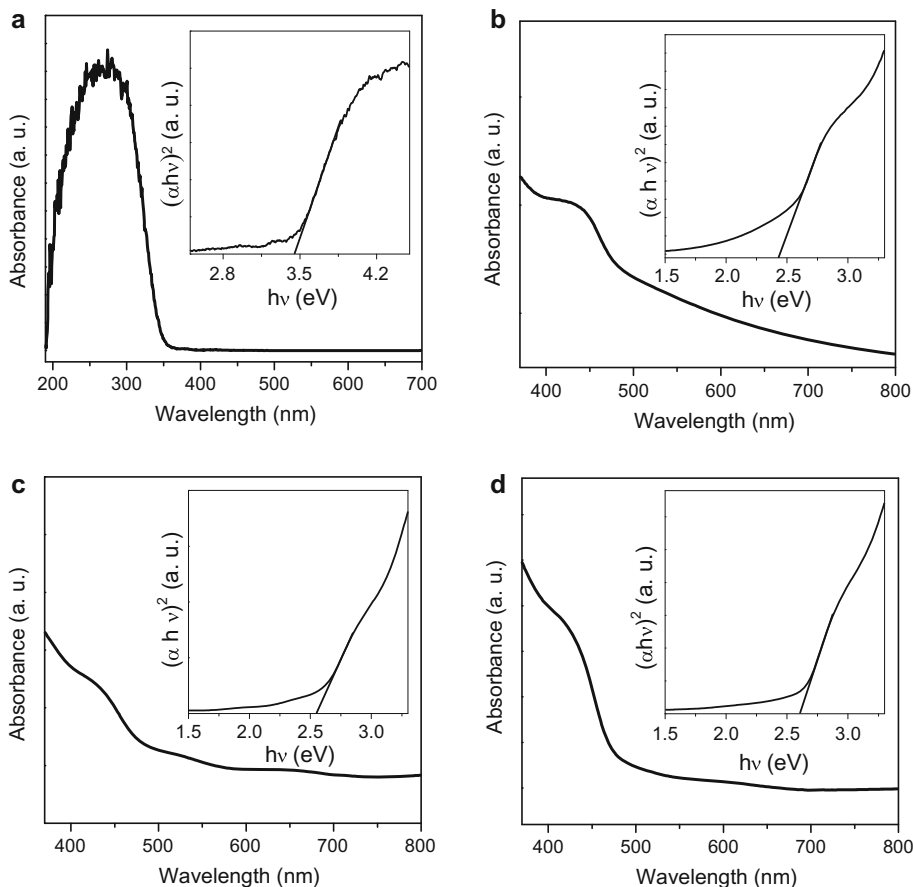
Fig. 7 UV–VIS spectra of methylene blue solution in 0.1 mol L^{-1} KCl after degradation reaction using different electrodes: **a** single BiVO$_4$, **b** n-BiVO$_4$/p-NiO and **c** p-NiO/n-BiVO$_4$. **d** Decay curves of methylene blue concentrationas function of degradation time
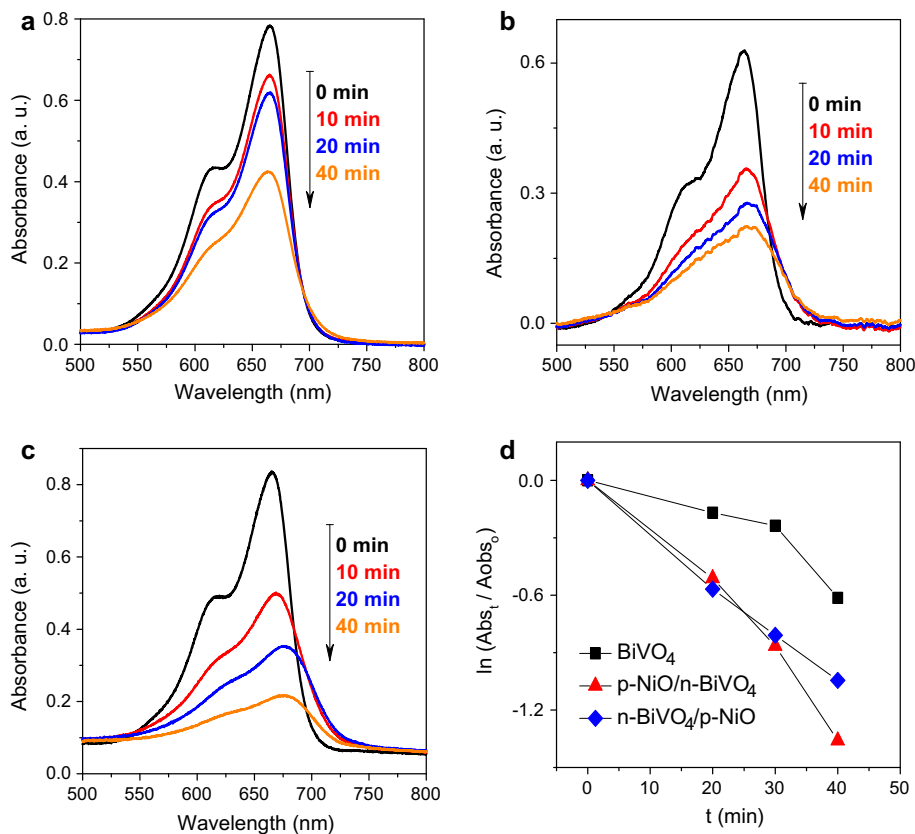

Table 1 Bandgap energy and kinetic parameters (k_{obs} and degradation at 40 min) obtained from pure BiVO$_4$ and n-BiVO$_4$/p-NiO and p-NiO/n-BiVO$_4$ heterojunction electrodes

	Bandgap (eV)	Degradation at 40 min (%)	k_{obs} min^{-1}
BiVO$_4$	2.42	45	150×10^{-4}
p-NiO-/n-BiVO$_4$	2.55	75	340×10^{-4}
n-BiVO$_4$/p-NiO	2.59	65	270×10^{-4}

respectively), E^e is the energy of free electrons on the hydrogen scale (~ 4.5 eV) and E$_g$ is the band gap energy of the semiconductor (E$_g$ are 2.4 and 3.4 eV for BiVO$_4$ and NiO [35], respectively). According to empirical Eqs. (1) and (2), E$_{VB}$ and E$_{CB}$ estimated values of BiVO$_4$ correspond to 2.75 and 0.33 eV versus Ag/AgCl, respectively. To the NiO semiconductor, E$_{VB}$ and E$_{CB}$ estimated values correspond to 3.13 and -0.31 eV, respectively. From these band-edge potential positions, a schematic energy diagram of charge transfer between p-type and n-type semiconductors, was constructed and can be seen in Fig. 8b. In the FTO/p-NiO/n-BiVO$_4$ electrode configuration (meaning BiVO$_4$ deposited on NiO), the electrode surface is formed of a higher concentration of BiVO$_4$ particles (yellow circles) along with a few disperse NiO particles (represented by the gray color in the background), as observed in

Fig. 8a. Then, under visible light irradiation from the dichroic lamp source, electron–hole pairs are generated in the BiVO$_4$ surface, as shown by vertical green arrow in Fig. 8b. Simultaneously, part of visible light radiation of smaller energy (higher wavelength) cause a simple excitation of valence band electrons to the Ni^{2+} vacancy level which is an acceptor trap (represented by A$^-$ in Fig. 8b with green color), since there is not energy enough for generation of electron–hole pairs in this material [34]. In this case, an increase in the holes density is obtained in the valence band of NiO. Thus, these holes are injected on valence band of BiVO$_4$, since holes tend to float, and the valence band-edge potential position is lower for NiO compared to BiVO$_4$. Then, the BiVO$_4$ surface-photogenerated holes lead to the generation of $^\bullet$OH type radicals, through water oxidation, which is a fundamental aspect in processes of MB degradation, related to the attack to the chromophore group of this molecule [7, 9, 48, 49]. Then, the overall result is a suppression of electron–hole pair recombination process, because electrons and holes stay in different regions of the device: the photogenerated electrons from the conduction band of BiVO$_4$ are injected in the Ni^{2+} vacancy level of NiO, due to the effect of the inner electric field, and the holes, coming from the valence band of NiO are injected on the valence band of BiVO$_4$, reacting with MB at device surface, as shown in Fig. 8b. In
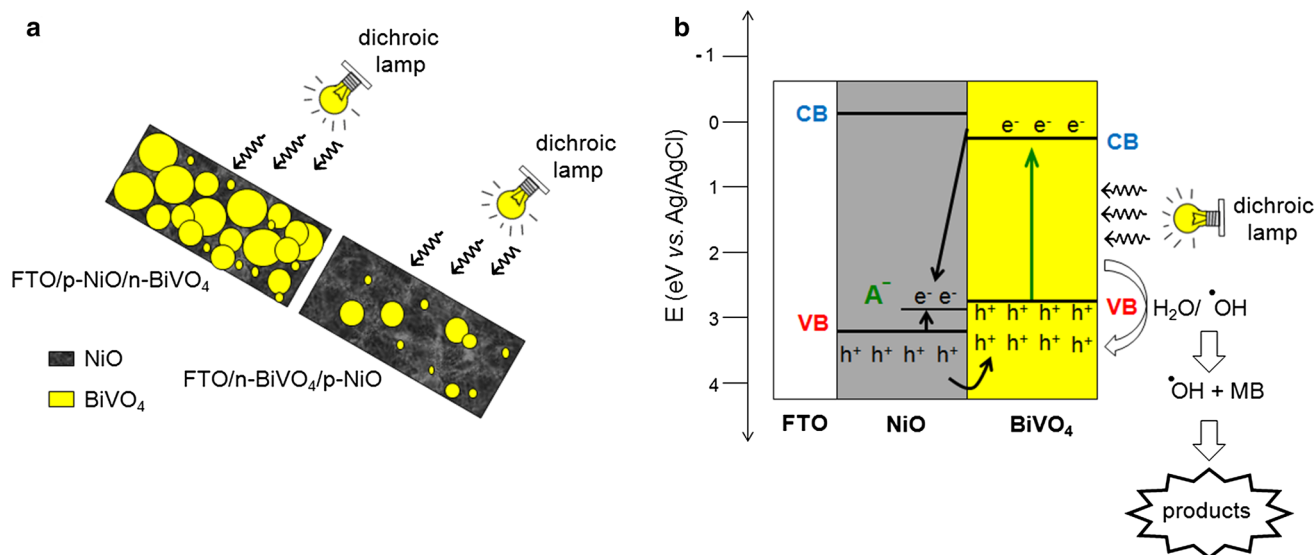
Fig. 8 **a** Schematic drawing illustrating the distinct concentration of $BiVO_4$ and NiO materials depending on the deposition order, and the p–n junctions formed on film surface. **b** Schematic diagram of charge transfer between p-type NiO and n-type $BiVO_4$

order to maintain the heterojunction overall charge neutrality, electrons from NiO and $BiVO_4$ materials, not trapped at Ni^{2+} vacancy defect levels, are injected into the FTO substrate and transferred to the counter-electrode, by the electrochemical bias applied to the system, where a chemical reduction reaction occurs. Then, the $BiVO_4$ particles on film surface, as shown by illustrative drawing in the Fig. 8a, are the reactive centers of p–n junction film.

In the other hand, in the FTO/n-$BiVO_4$/p-NiO electrode configuration (meaning NiO deposited on $BiVO_4$), although the same effect is observed, the efficiency in MB degradation is a rather lower, as shown by the kinetic parameters exhibit in Table 1. This effect is due to the concentration of reactive centers available on the film surface, the $BiVO_4$ particles, which is lower in this case, when compared to FTO/p-NiO/n-$BiVO_4$ electrode configuration.

4 Conclusion

The obtained results of XRD, SEM, UV–Vis optical spectroscopy and Raman spectroscopy have shown that the precipitation in an aqueous medium and solution combustion synthesis techniques concomitant with the dip-coating deposition process leads to interpenetrating film layers of $BiVO_4$ and NiO, as p–n heterojunctions, which are very efficient for methylene blue degradation in photoelectro-catalysis processes, compared to the single $BiVO_4$ thin film. The performance analysis have also shown that the p–n electrodes, FTO/NiO/$BiVO_4$ (meaning $BiVO_4$ deposited on top of NiO) have better efficiency and higher electroactivity for MB degradation when compared to FTO/

$BiVO_4$/NiO (meaning NiO deposited on top of $BiVO_4$), under visible light irradiation condition, with estimated k_{obs} value of 340×10^{-4} min^{-1} and 270×10^{-4} min^{-1}, respectively. This performance is explained by a simple model, taking into account the relative position of energy bands and photo-induced free carries move.

The investigation presented in this paper shows that, although the phase mixtures on the top layer is not a desirable result for electronic applications, it is quite interesting for decontamination procedures. The methylene blue degradation results reveal that this sort of heterostructure, within a specific architecture, emerges as a potential electrode material that can be used in a real situation in decontaminating wastewater.

References

1. M. Faisal, S. Khan, M.M. Rahman, A.A. Ismail, A.M. Asiri, S.A. Al-Sayari, J. Taiwan Inst. Chem. E **45**, 2733 (2014)
2. M. Constapel, M. Schellentrager, J.M. Marzinkowski, S. Gäb, Water Res. **43**, 733 (2009)
3. L. Wen, B. Liu, X. Zhao, K. Nakata, A. Fujishima, J. Electroanal. Chem. **688**, 224 (2013)
4. E.R.A. Ferraz, G.A.R. Oliveira, M.D. Grando, T.M. Lizier, M.V.B. Zanoni, D.P. Oliveira, J. Environ. Manag. **124**, 108 (2013)
5. M. Fan, C. Yang, W. Pu, J. Zhang, Mat. Sci. Semicond. Proc. **17**, 104 (2014)
6. Z. Li, F. Gao, W. Kang, Z. Chen, M. Wu, L. Wang, D. Pan, Mater. Lett. **97**, 52 (2013)

7. M.R. Silva, L.H. Dall'Antonia, L.V.A. Scalvi, D.I. Santos, L.O. Ruggiero, A. Urbano, J. Solid State Electrochem. **16**, 2016 (2012)

8. L.H. Dall' Antonia, N.R. Tacconi, W. Chanmanee, H. Timmaji, N. Myung, K. Rajeshwar, Electrochem. Solid State **13**, D29 (2010)

9. H.K. Timmaji, W. Chanmanee, N.R. Tacconi, K. Rajeshwar, J. Adv. Oxid. Technol. **14**, 1495 (2011)

10. G. Du, Y. Cui, X.C. Xia, X.P. Li, H.C. Zhu, B.L. Zhang, Y.T. Zhang, Y. Ma, Appl. Phys. Lett. **90**, 243504 (2007)

11. S.T. Tan, J.L. Zhao, S. Iwan, X.W. Sun, X. Tang, J. Ye, M. Bosman, L.J. Tang, G.Q. Lo, K.L. Teo, IEEE Trans. Electron Dev. **57**, 129 (2010)

12. J.L.B. Maciel, E.A. Floriano, L.V.A. Scalvi, L.P. Ravaro, J. Mater. Sci. **46**, 6627 (2011)

13. D.C. Tsui, Phy. Rev. Lett. **24**, 303 (1970)

14. C.W. Bark, P. Sharma, Y. Wang, S.H. Beak, S. Lee, S. Ryu, C.M. Folkman, T.R. Paudel, A. Kumar, S.V. Kalinin, A. Sokolov, E.Y. Tsymbal, M.S. Rzchowski, A. Gruverman, C.B. Eom, Nano Lett. **12**, 1765 (2012)

15. Y. Wang, M.K. Niranjan, S.S. Jaswal, E.Y. Tsymbal, Phy. Rev. B **80**, 165130 (2009)

16. H.W. Jang, D.A. Felker, C.W. Bark, Y. Wang, M.K. Niranjan, C.T. Nelson, Y. Zhang, D. Su, C.M. Folkman, S.H. Baek, S. Lee, K. Janicka, Y. Zhu, X.Q. Pan, D.D. Fong, E.Y. Tsymbal, M.S. Rzchowski, C.B. Eom, Science **331**, 886 (2011)

17. T.F. Pineiz, L.V.A. Scalvi, M.J. Saeki, E.A. Morais, J. Electron. Mater. **39**, 1170 (2010)

18. T.F. Pineiz, E.A. Morais, L.V.A. Scalvi, C.F. Bueno, Appl. Surf. Sci. **267**, 200 (2013)

19. J.S. Jang, H.G. Kim, S.-H. Lee, J. Phys. Chem. Solids **73**, 1372 (2012)

20. J. Zhang, H. Cui, B. Wang, C. Li, J. Zhai, Q. Li, Appl. Surf. Sci. **300**, 51 (2014)

21. L. Zhang, G. Tan, S. Wei, H. Ren, A. Xia, Y. Luo, Ceram. Int. **39**, 8597 (2013)

22. S. Xie, T. Zhai, Y. Zhu, W. Li, R. Qiu, Y. Tong, X. Lu, Int. J. Hydrogen Energy **39**, 4820 (2014)

23. J. Jiang, M. Wang, R. Li, L. Ma, L. Guo, Int. J. Hydrogen Energy **38**, 13069 (2013)

24. I. Fujimoto, N. Wang, R. Saito, Y. Miseki, T. Gunji, K. Sayama, Int. J. Hydrogen Energy **39**, 2452 (2014)

25. H. Li, W. Hong, Y. Cui, X. Hu, S. Fan, L. Zhu, Mater. Sci. Eng. B Adv. **181**, 1 (2014)

26. M. Wang, Y. Che, C. Niu, M. Dang, D. Dong, J. Hazard. Mater. **262**, 447 (2013)

27. W. Wang, X. Huang, S. Wu, Y. Zhou, L. Wang, H. Shi, Y. Liang, B. Zou, Appl. Catal. B Environ. **134–135**, 293 (2013)

28. S. Tokunaga, H. Kato, A. Kudo, Chem. Mater. **13**, 4624 (2001)

29. R. Afonso, J.A. Serafim, A.C. Lucilha, M.R. Silva, L.F. Lepre, R.A. Ando, L.H. Dall'Antonia. J. Braz. Chem. Soc. **25**, 726 (2014)

30. J.A. Serafim, R. Afonso, A.C. Lucilha, L.A. Oliveira, P.R.C. Silva, M.R. Silva, E.R. Sartori, L.H. Dall'Antonia, Quim. Nova **37**, 1158 (2014)

31. K. Rajeshwar, N.R. Tacconi, Chem. Soc. Rev. **38**, 1984 (2009)

32. S.-F. Wang, L.-Y. Shi, X. Feng, S.-R. Ma, Mater. Lett. **61**, 1549 (2007)

33. Q.Y. Li, R.N. Wang, Z.R. Nie, Z.H. Wang, Q. Wei, J. Colloid Interface Sci. **320**, 254 (2008)

34. M.R. Silva, L.V.A. Scalvi, L.H. Dall'Antonia, D.I. Santos, J. Mater. Sci. Mater. Electron. **24**, 1823 (2013)

35. M.R. Silva, A.C. Lucilha, R. Afonso, L.H. Dall'Antonia, L.V.A. Scalvi, Ionics **20**, 105 (2014)

36. X. Zhang, S. Chen, X. Quan, H. Zhao, Sep. Purif. Technol. **64**, 309 (2009)

37. Y.K. Kho, W.Y. Teoh, A. Iwase, L. Madler, A. Kudo, R. Amal, Appl. Mater. Interfaces **3**, 1997 (2011)

38. N. Mironova-Ulmane, A. Kuzmin, I. Sildos, M. Pärs, Cent. Eur. J. Phys. **9**, 1096 (2011)

39. M. Marciuš, M. Ristic, M. Ivanda, S. Music, J. Alloys Compd. **541**, 238 (2012)

40. N. Mironova-Ulmane, V. Skvortsova, A. Kuzmin, U. Ulmani, I. Sildos, E. Cazzanelli, G. Mariotto, Phy. Solid State **47**, 1516 (2005)

41. S.H. Lee, H.M. Cheong, N.G. Park, C.E. Tracy, A. Mascarenhas, D.K. Benson, S.K. Deb, Solid State Ion. **140**, 135 (2001)

42. V. Gowthami, P. Perumal, R. Sivakumar, C. Sanjeeviraja, Phys. B **452**, 1 (2014)

43. C. Xu, G. Xu, G. Wang, J. Mater. Sci. **38**, 779 (2002)

44. A. Hakim, J. Hossain, K.A. Khan, Renew. Energy **34**, 2625 (2009)

45. W. Zhao, Y. Wang, Y. Yang, J. Tang, Y. Yang, Appl. Catal. B Environ. **115–116**, 90 (2012)

46. M.-L. Guan, D.-K. Ma, S.-W. Hu, Y.-J. Chen, S.-M. Huang, Inorg. Chem. **50**, 800 (2011)

47. X. Chen, S. Shen, L. Guo, S.S. Mao, Chem. Rev. **110**, 6503 (2010)

48. S. Naya, M. Tanaka, K. Kimura, H. Tada, Langmuir **27**, 10334 (2011)

49. H.-Q. Jiang, H. Endo, H. Natori, M. Nagai, K. Kobayashi, J. Eur. Ceram. Soc. **28**, 2955 (2008)